9,400 years of cosmic radiation and solar activity from ice cores and tree rings

Friedhelm Steinhilber[a,1], Jose A. Abreu[a2], Jürg Beer[a], Irene Brunner[a], Marcus Christl[b], Hubertus Fischer[c], Ulla Heikkilä[d], Peter W. Kubik[b], Mathias Mann[a], Ken G. McCracken[e], Heinrich Miller[f], Hiroko Miyahara[g], Hans Oerter[f], and Frank Wilhelms[f]

[a]Swiss Federal Institute of Aquatic Science and Technology, Eawag, Überlandstrasse 133, 8600 Dübendorf, Switzerland; [b]Laboratory of Ion Beam Physics, Swiss Federal Institute of Technology Zurich, Schafmattstrasse 20, 8093 Zurich, Switzerland; [c]Climate and Environmental Physics, Physics Institute and Oeschger Centre for Climate Change Research, University of Bern, Sidlerstrasse 5, 3012 Bern, Switzerland; [d]Ulla Heikkilä, Australian Nuclear Science and Technology Organisation (ANSTO), Lucas Heights, North South Wales 2234, Australia; [e]Ken G. McCracken, Institute for Physical Science and Technology, University of Maryland, College Park, MD 20742; [f]Alfred Wegener Institute for Polar and Marine Research, Am Handelshafen 12, 27568 Bremerhaven, Germany; and [g]Institute for Cosmic Ray Research, University of Tokyo, 5-1-5 Kashiwanoha, Kashiwa 277-8582, Japan

Edited by Timothy Patterson, Carleton University, and accepted by the Editorial Board February 14, 2012 (received for review November 18, 2011)

Understanding the temporal variation of cosmic radiation and solar activity during the Holocene is essential for studies of the solar-terrestrial relationship. Cosmic-ray produced radionuclides, such as ^{10}Be and ^{14}C which are stored in polar ice cores and tree rings, offer the unique opportunity to reconstruct the history of cosmic radiation and solar activity over many millennia. Although records from different archives basically agree, they also show some deviations during certain periods. So far most reconstructions were based on only one single radionuclide record, which makes detection and correction of these deviations impossible. Here we combine different ^{10}Be ice core records from Greenland and Antarctica with the global ^{14}C tree ring record using principal component analysis. This approach is only possible due to a new high-resolution ^{10}Be record from Dronning Maud Land obtained within the European Project for Ice Coring in Antarctica in Antarctica. The new cosmic radiation record enables us to derive total solar irradiance, which is then used as a proxy of solar activity to identify the solar imprint in an Asian climate record. Though generally the agreement between solar forcing and Asian climate is good, there are also periods without any coherence, pointing to other forcings like volcanoes and greenhouse gases and their corresponding feedbacks. The newly derived records have the potential to improve our understanding of the solar dynamics and to quantify the solar influence on climate.

cosmogenic radionuclides | cosmic rays | solar modulation

Most of the cosmic ray particles reaching the Earth are produced outside the solar system during supernova explosions. Mainly two magnetic shields, the solar magnetic field and the geomagnetic field, modulate the cosmic ray flux approaching the Earth. Both shields vary in time, and so does the cosmic radiation at Earth. The weaker these fields, the higher is the cosmic ray intensity at Earth. Ionization chambers and neutron monitors have directly monitored the intensity of cosmic radiation since the 1930s (1). Prior to this time, no direct measurements exist, and cosmogenic radionuclides, which can be considered as a kind of a "natural neutron monitor," can be used as a proxy for cosmic radiation (2). In this context the two most commonly used radionuclides are ^{10}Be and ^{14}C. ^{10}Be and ^{14}C are produced in the Earth's atmosphere by nuclear reactions of cosmic ray particles with atmospheric nitrogen and oxygen (3) (Fig. 1). Thus, the production rates of these nuclides are directly related to the flux of the incoming cosmic ray particles. Although their production processes are very similar, their geochemical behavior in the Earth system is completely different (Fig. 1). ^{14}C enters the global carbon cycle, and therefore fluctuations of the atmospheric ^{14}C concentration (Fig. 2*B*) measured as Δ^{14}C in tree rings are damped, smoothed, and delayed relative to the ^{14}C production. The effect of the carbon cycle can be removed by inverse carbon cycle modeling. The resulting ^{14}C production rate (p^{14}C, Fig. 2 *C* and *D*) calculated with a box-diffusion carbon cycle model (4) is a better measure of the cosmic radiation, but it still contains a climate signal component due to unknown temporal changes of the carbon cycle and a memory effect of the production history. In contrast to ^{14}C, aerosol-borne ^{10}Be is removed from the atmosphere relatively fast within a few years and stored in natural archives such as polar ice sheets. Because of its short atmospheric residence time, ^{10}Be directly reflects cosmic ray intensity variations with almost no attenuation and a delay of 1–2 y. Uncertainties are introduced mainly on annual time scales by atmospheric mixing processes and wet and dry deposition from the atmosphere to the ice (5).

For the Holocene there are several radionuclide records with high temporal resolution: p^{14}C (Fig. 2 *C* and *D*) derived from Δ^{14}C measured in tree rings (Fig. 2*B*), and ^{10}Be from different ice cores from Greenland and Antarctica (Fig. 2 *A* and *D*). The high similarity between the two different radionuclides ^{14}C and ^{10}Be and the fact that the well known grand solar minima such as the Maunder and the Dalton minima are well represented in the radionuclide records (Fig. 2*D*) confirms that these records reflect primarily production changes caused by variations of the cosmic ray flux. However, closer inspection reveals that often, the shapes during these periods differ slightly in their details. Because the cosmic ray induced production changes are almost identical for ^{10}Be and ^{14}C, the differences observed in radionuclide records stored in geological archives are the result of so-called system effects. The term "system effects" is used here for all processes influencing the radionuclide signal (e.g., climate-induced transport and deposition changes, changes in the carbon cycle) other than cosmic ray-induced production (heliomagnetic and geomagnetic modulation). A prominent system effect, for example, is the variation of the snow accumulation rate, which directly affects the ^{10}Be concentration stored in the ice. To some extent system effects can be corrected. For example, snow accumulation effects can be partly removed by calculating ^{10}Be fluxes (concentration times snow accumulation rate). However, due to the combination of both wet and dry deposition on the total aerosol deposition, neither concentration nor fluxes are truly independent of accumulation rate (6). The determination of the snow accumulation

Author contributions: J.B. designed research; F.S., J.A.A., J.B., M.M., U.H., and K.G.M. performed research; F.S., H.F., H. Miller, H. Miyahara, H.O., and F.W. contributed new reagents/analytic tools; F.S., J.A.A., J.B., I.B., M.C., U.H., P.W.K., and M.M. analyzed data; and F.S. wrote the paper.

The authors declare no conflict of interest.

This article is a PNAS Direct Submission. T.P. is a guest editor invited by the Editorial Board.

[1]To whom correspondence should be addressed. E-mail: friedhelm.steinhilber@eawag.ch.

[2]Present address: Earth and Planetary Magnetism Group, Swiss Federal Institute of Technology Zurich, Institute of Geophysics, Sonneggstrasse 5, 8092 Zurich, Switzerland.

This article contains supporting information online at www.pnas.org/lookup/suppl/doi:10.1073/pnas.1118965109/-/DCSupplemental.

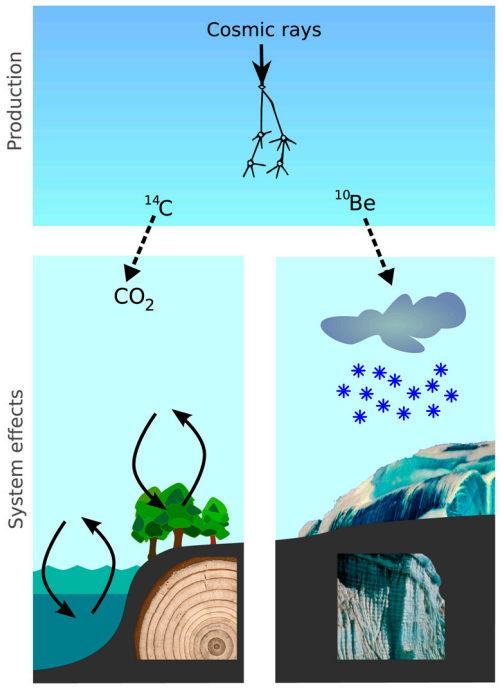

Fig. 1. Cartoon illustrating some basics of the radionuclides ^{14}C and ^{10}Be in the Earth's system. Both radionuclides are produced in a very similar way by nuclear reactions of cosmic ray particles with the atmospheric gases (3). After production, their fate is very different (system effects). ^{10}Be attaches to aerosols and is transported within a few years to ground (34). ^{14}C oxidizes to CO_2 and enters the global carbon cycle, exchanging between atmosphere, biosphere, and the oceans (4).

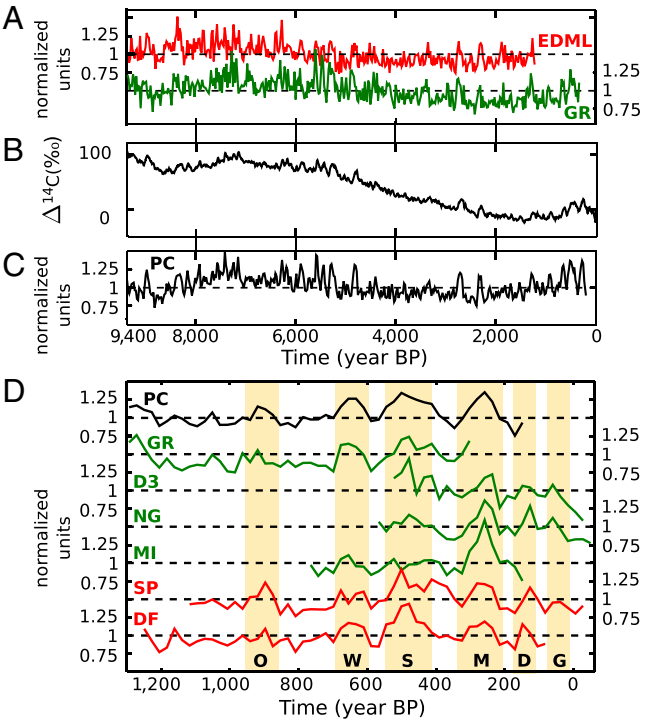

Fig. 2. Radionuclide records used for this study. ^{10}Be concentration records are green (Greenland) and red (Antarctica) and ^{14}C is black. Time is given as year before present (BP where present refers to 1950 AD). All records are mean normalized (divided by the mean) 22-year averages. (*A*) New ^{10}Be record from the EDML ice core (red) and of the existing ^{10}Be record from the GRIP (GR) ice core (green). The data are plotted on the time scales EDML1 (35) for EDML and GICC05 (36, 37) for GRIP. (*B*) $\Delta^{14}C$, the deviation of the atmospheric $^{14}C/^{12}C$ ratio from a standard value, measured in tree rings (14) and (*C*) ^{14}C production rate $p^{14}C$ (PC), calculated with a box-diffusion carbon cycle model (4) from $\Delta^{14}C$ (14) over the last 9,400 y. (*D*) ^{14}C production rate $p^{14}C$ (PC) and ^{10}Be concentrations for several available ice cores (GR: GRIP; D3: Dye-3; NG: NorthGRIP; MI: Milcent; SP: South Pole; DF: Dome Fuji) over the last 1,200 y. Grand solar minima are marked by yellow bands and capital letters: O: Oort, W: Wolf, S: Spörer, M: Maunder, D: Dalton, G: Gleissberg.

rate of an ice core is not trivial and is associated with additional uncertainties. In the polar regions of Greenland and Antarctica, snow accumulation rates have been rather stable during the Holocene so that ^{10}Be concentrations and fluxes yield similar results (*SI Appendix*, Section S7). For the sake of simplicity we use the concentrations below.

From this discussion it is obvious that individual radionuclide records may contain a significant system component which, if not eliminated, would be incorrectly attributed to variations of the cosmic radiation. In fact, system effects are probably the main reason for the observed differences between the existing reconstructions of cosmic radiation based on single radionuclide records only (7–10).

Results

Here we present a cosmic ray record for the past 9,400 y for which the system effects were minimized. This high-resolution and low-noise paleocosmic ray record is used to derive solar activity that in turn provides a powerful tool to search for the solar fingerprint in climate records.

Our approach first combines several hemispheric ^{10}Be records with the global ^{14}C record with high temporal resolution (Fig. 2 *A*, *C*, and *D* and Table 1) and then follows the study of Abreu, et al. (11) by using principal component analysis (PCA) to extract the common production signal. With PCA it is possible to disentangle the cosmic ray-induced production signal from the system effects. The successful separation is based on the assumption that the production signal is common to all records (correlated), whereas the system effects are different (uncorrelated) in each record. If system effects affected the radionuclide records spatially and temporarily in a similar way, PCA would "misinterpret" these effects as common variation which in turn would be wrongly attributed to cosmic radiation changes. However, it is known that climate effects differ spatially; hence it seems justified to assume that they affect the different radionuclide records from different hemispheres and archives differently.

The three main records of our reconstruction [^{10}Be from European Project for Ice Coring in Antarctica-Dronning Maid Land (EPICA-DML), Antarctica; ^{10}Be from European Greenland Ice Core Project (GRIP) (12, 13), Greenland; and global $p^{14}C$ from tree rings (14)] represent both hemispheres and are measured in different archives. These three records cover a time range from 1,194 to 9,400 y before present (BP) (*SI Appendix*, Section S1) and have a temporal resolution of a few years. The new ^{10}Be dataset from the EPICA-DML ice core consists of 1,846 data points with an average temporal resolution of about 4.5 y and therefore provides an essential part for the reconstruction. To homogenize the different records, 22-year averages are calculated for each individual record. Then PCA is applied to the 22-year averages. The first principal component explains 69% of the total variance (*SI Appendix*, Section S6). This is a striking result because it implies that the ^{14}C production changes throughout the Holocene are very similar to the ^{10}Be changes found in polar ice cores from the two different hemispheres. Again, because ^{10}Be and ^{14}C are produced in a very similar way and because system effects are not expected to correlate with the production signal, we conclude that the first principal component is the best representation of the global production rate and herewith of the cosmic ray intensity at Earth. The production signal obtained from ^{10}Be from GRIP and EPICA Dronning Maud

Table 1. Radionuclide records used in the study and their characteristics (3)

Record	Nuclide	Source	Time span (year before present)	Mean value used to normalize data in Fig. 2 (10^4 atoms/g)	Reference
INTCAL09	^{14}C	tree rings	9,400 to 150	1*	(14)
EDML†	^{10}Be	ice Antarctica	9,400 to 1,200	4.1	New
GRIP ‡	^{10}Be	ice Greenland	9,400 to 300	1.5	(12), (13)
Dye-3	^{10}Be	ice Greenland	526 to −35	1.1	(16)
Milcent	^{10}Be	ice Greenland	769 to 148	1.1	(17)
NorthGRIP	^{10}Be	ice Greenland	561 to −44	1.8	(15)
South Pole	^{10}Be	ice Antarctica	1,107 to −32	3.8	(19)
Dome Fuji	^{10}Be	ice Antarctica	1,255 to 75	9.4	(18)

*The ^{14}C production rate in the carbon cycle model is 1 (idealized units) for present day ($\Delta^{14}C = 0‰$). The global average ^{14}C production is approximately 2 atoms cm^{-2} s^{-1} (3).

†European Project for Ice Coring in Antarctica Dronning Maud Land area

‡European Greenland Ice Core Project

Land area (EDML) ice cores and ^{14}C from tree rings for the period 1,194–9,400 BP is extended to the present day by applying PCA to several other high-resolution ^{10}Be records from Greenland [NorthGRIP (15), Dye3 (16), Milcent (17)] and Antarctica [Dome Fuji (18), South Pole (19)], and to ^{14}C from tree rings (14). In this time interval the production signal is also dominant, explaining more than 67% of the total variance. The entire record is normalized to the two most recent 22-year averages centered in 1955 and 1977 AD (*SI Appendix*, Section S9). By combining several radionuclide records with PCA as done in this study, an assessment of the systematic uncertainty can be done. The common signal in radionuclide records describes about 70% of the variance, implying that the system effects cause the remaining 30%. These system effects are removed by using only the first principal component. The robustness of PCA was tested by applying a jackknife method, applying PCA to subsets of radionuclide records by leaving out single records. The jackknife uncertainty is on average 5% (*SI Appendix*, Section S8), which is significantly smaller than the large (greater than 50%) variations due to changes in solar activity between periods of low solar activity like the Maunder minimum (20) and of high solar activity like the past decades.

We note that there are several sources of systematic error that are not removed by PCA. These are (*i*) uncertainties in the time scales of the individual records, (*ii*) uncertainties in the production rate calculations of ^{10}Be and ^{14}C, (*iii*) the assumption that relative variations of ^{10}Be concentrations and ^{10}Be production rates are equal, (*iv*) uncertainty in the assumption of linear independence between production and system effects.

Variations on different time scales are evident in the final low-noise cosmic radiation (radionuclide production) record (Fig. 3 *B*, *C*, and *D*). A comparison with changes in the geomagnetic dipole field strength (21) (Fig. 3*A*) shows that the geomagnetic dipole shielding is the main cause of the observed multimillennial variability; the stronger the geomagnetic field, the lower is the cosmic radiation. On multidecadal to centennial time scales the cosmic radiation variations are mostly due to solar modulation (Fig. 3 *C* and *D*) as indicated by the coincidence of cosmic radiation maxima and grand solar (sunspot) minima like the Maunder minimum (Fig. 3*D*).

In a second step, we use the new low-noise cosmic radiation record to reconstruct total solar irradiance (TSI) by first removing the shielding effect of the geomagnetic field (3) (Fig. 3*A*) and then applying the procedure described in refs. 22–24 (*SI Appendix*, Section S10). The wavelet coherence between TSI of this study and two other recent TSI reconstructions (22, 25) based on single radionuclide records show agreement in the low-frequency part (periods longer than 100 y) and differences in the high-frequency part (periods shorter than 100 y) (*SI Appendix*, Section S13). This finding indicates that the PCA has indeed reduced the high-frequency noise present in the individual single radionuclide records.

In a last step, TSI is compared with the δ^{18}O record from Dongge cave, China, supposedly reflecting variations in precipitation amount related to changes in the Asian monsoon (AM) (26) (Fig. 4).

Note, however, that a recent climate modeling study (27) did not find a correlation between δ^{18}O in Chinese precipitation and the amount of precipitation over the Holocene. However, the study (27) showed that changes in monsoon are related to changes in δ^{18}O, although not via variations in the amount of precipitation.

Climate records have been often compared with Δ^{14}C as a proxy of solar activity. The Dongge Cave record has been previously compared with Δ^{14}C (21). As discussed above, Δ^{14}C is

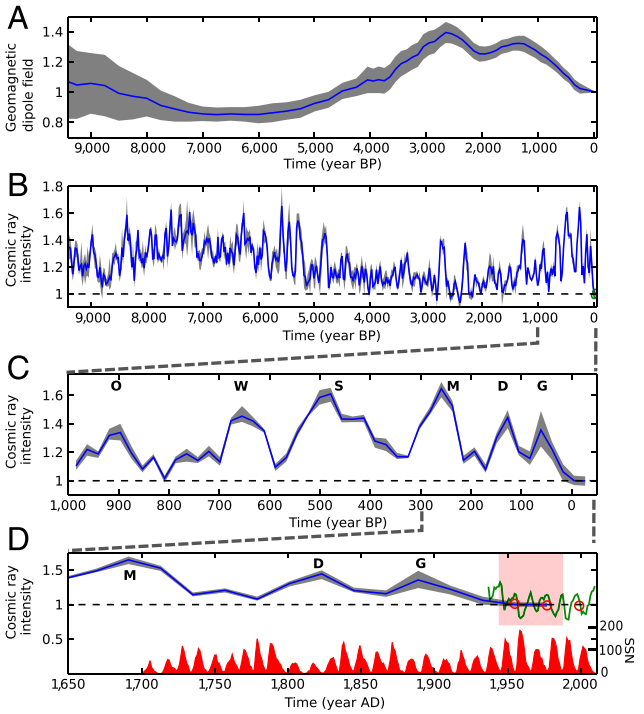

Fig. 3. (*A*) Geomagnetic dipole field strength relative to today (21). (*B*) Cosmic radiation based on the first principal component of several radionuclide records, 22-year averages, over the last 8,000 y. Time is given as year BP. The gray band represents the standard deviation of the individual radionuclide records without applying PCA (*SI Appendix*, Section S8). The black dashed line represents the average cosmic ray intensity for 1944–1988 AD. (*C*) Same as (*B*), but zoom-in of the past millennium. Capital letters mark grand solar minima: O: Oort, W: Wolf, S: Spörer, M: Maunder, D: Dalton, G: Gleissberg. (*D*) Same as (*C*), but zoom-in of the past 350 y. Time is given as year AD. Red circles and green curve are 22-year averages and yearly averages of cosmic ray intensity calculated with (3) using the solar modulation potential (38) obtained from neutron monitor and ionization chamber data (*SI Appendix*, Section S9). At the bottom the annual sunspot number is plotted (39).

not directly showing the solar forcing signal but a solar and geomagnetic production signal filtered by the carbon cycle system, which leads to a frequency dependent attenuation of the amplitude and a phase shift. Thus, a repetition using the solar activity record derived in our study appears to be justified. This climate record was chosen for two reasons: First, it is one of the few accurately dated climate records with high resolution that covers a similar period as the derived TSI. Second, it is a good example to demonstrate how to detect a solar signal in a climate record. The climate record has a large long-term trend due to orbital forcing, which we removed by subtracting the linear trend and applying a 2,000-year high-pass filter. We used the same data processing (subtracting the linear trend and applying a 2,000-year high-pass filter) for TSI.

We emphasize that changes in TSI are phase-locked with changes in solar spectral irradiance and with other changes related with solar activity, and therefore here we cannot distinguish between these different solar forcings. Hence, in this context TSI is taken as a proxy of solar activity, which is the reason we use the term solar activity instead of TSI in the following discussion.

The Pearson correlation between solar activity and AM is $R = -0.29$, meaning, during periods of low solar activity the AM strength has been weaker (higher $\delta^{18}O$) (Fig. 4*A*). Despite being significantly different from zero ($p < 10^{-6}$), this correlation, however, can only explain 10% in the total decadal to centennial variance in the AM record. We did a correlation analysis and found that the strongest correlation is found for a slightly negative lag (22 y), which is consistent with no lag within the uncertainty (*SI Appendix*, Section S12). The power spectrum of solar activity (*SI Appendix*, Section S11) shows significant periodicities ($p < 0.05$) already known from individual ^{14}C and ^{10}Be records such as the de Vries cycle (around 210 y), the Eddy cycle (around 1,000 y) (28), and an unnamed cycle at approximately 350 y, as well as other less significant unnamed cycles at approximately 500 and 710 y. These periodicities, although not significant, are also found in the Asian climate (*SI Appendix*, Section S11). The wavelet spectrum of solar activity (Fig. 4*B*) shows that the amplitudes

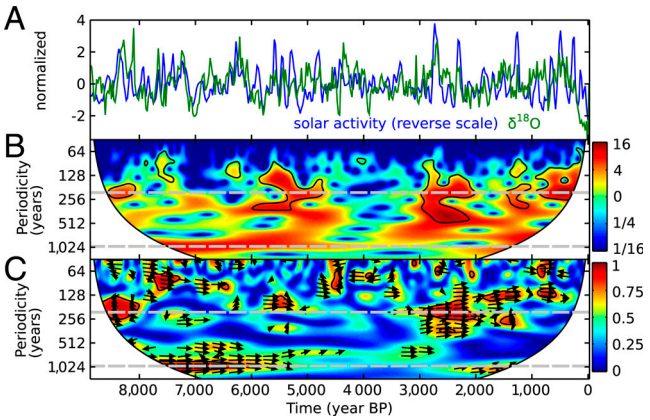

Fig. 4. Comparison of solar activity (total solar irradiance [TSI]) in blue and $\delta^{18}O$ from Dongge cave, China, in green representing changes of the Asian climate. possibly the Asian monsoon (AM) (low $\delta^{18}O$ corresponds to strong AM monsoon and vice versa). TSI has been reconstructed from the cosmic ray intensity reconstruction (*SI Appendix*, Section S10). Both records have been normalized (subtraction of mean value and division by the standard deviation), linearly detrended and high-pass filtered with 2,000 y. (*A*) Time series of solar activity (TSI) and $\delta^{18}O$. Solar activity (TSI) is plotted on a reversed scale. (*B*) Wavelet of solar activity (TSI). De Vries cycle at approximately 210 y and Eddy cycle at approximately 1,000 y are marked with horizontal, gray dashed lines. Black boundaries mark 95% significance level. (*C*) Wavelet coherence of solar activity (TSI) and $\delta^{18}O$. De Vries cycle at approximately 210 y and Eddy cycle at approximately 1,000 y are marked with horizontal, gray dashed lines. Arrows pointing to the right indicate that the records are in phase. Black boundaries mark the 95% significance level.

of these periodicities have varied in time, that is, the de Vries cycle amplitude has varied with a period of about 2,200 y, called the Hallstatt cycle (29). The largest amplitudes of the de Vries cycle are found during Hallstatt cycle minima centered at approximately 8,200; 5,500; 2,500; and 500 BP. Comparison of the time series of solar activity and its wavelet spectrum (Fig. 4 *A* and *B*) show that grand solar minima occur preferentially at minima of the de Vries cycles (note that solar activity is plotted on a reversed scale in Fig. 4*A*). Comparison of the time series of solar activity and climate (Fig. 4*A*) and their wavelet coherence (Fig. 4*C*) shows that in general during the Hallstatt cycle minima of solar activity (again characterized by large de Vries cycle amplitudes and a frequent occurrence of grand solar minima) the AM is weaker. However, there is some discrepancy during the Hallstatt cycle minima between 5,000 and 6,000 BP and in the past 1,500 y. During these periods the wavelet coherence for the periodicity of the de Vries cycle (around 210 y) is low, although several grand solar minima are visible. A similar pattern is visible at the Eddy periodicity (around 1,000 y), which has high power in the wavelet coherence, except in the period 3,000 to 5,000 BP. Such temporal differences are expected because the Sun is not the only driver of the climate system. Other forcing factors such as volcanic aerosols and greenhouse gases have changed in time, obscuring temporally the solar fingerprint.

Conclusions

We combined a new ^{10}Be record from Dronning Maud Land, Antarctica, comprising more than 1,800 data points with several other already existing radionuclide records (^{14}C from tree rings and ^{10}Be analyzed in polar ice cores of Greenland and Antarctica) covering the Holocene. Using principal component analysis, we separated the common radionuclide production signal due to solar and geomagnetic activity from the system effects signal due to the different transport and deposition processes. The common signal represents a low-noise record of cosmic radiation, particularly for high frequencies, compared to earlier reconstructions, which are only based on single radionuclide records. On the basis of this record, we then derived a reconstruction of total solar irradiance for the Holocene, which overall agrees well with two existing records but shows less high-frequency noise. A comparison of the derived solar activity with a record of Asian climate derived from $\delta^{18}O$ in a Chinese stalagmite reveals a significant correlation. The correlation is remarkable because the Earth's climate has not been driven by the Sun alone. Other forcings like volcanoes, greenhouse gas concentrations, and internal variability also have played an important role. To quantify the solar influence on the Earth's climate and to distinguish between the different forcings, climate model simulations are required for the Holocene, employing the new dataset of total solar irradiance. The dataset will be available online at the National Oceanic and Atmospheric Administration paleo server (http://www.ncdc.noaa.gov/paleo/forcing.html).

Materials and Methods

Records Used in This Study. Table 1 summarizes the characteristics of the records used in this study. We applied a decay correction to the ^{10}Be records, using a half-life of (1.387 ± 0.012) million years (30, 31). The production rate p^{14}C from the atmospheric ^{14}C concentrations as measured in tree rings (14) has been calculated with a box-diffusion carbon cycle model (4).

^{10}Be EDML Record. The EDML ice core, located on the high plateau of the Atlantic sector of the East Antarctic ice sheet in Antarctic Dronning Maud Land, Antarctica, was drilled within the EPICA framework (32). The ^{10}Be record used covers the period from 1,193 to 9,400 BP. The chemical preparation of the ^{10}Be samples was done at Eawag in Dübendorf, Switzerland. First the ice was cut into samples of 25 cm length, corresponding to an average time resolution of about 4.5 y. Then the ice was melted in a microwave oven, mixed with 0.125 mg of ^{9}Be carrier, and passed through a cation ion exchange resin. The chemical preparation was done in the same way as for the ^{10}Be samples from the GRIP ice core (12, 13). The samples were measured

at the accelerator mass spectrometry (AMS) facility of Ion Beam Physics group at Swiss Federal Institute of Technology Zurich, Switzerland. The typical AMS uncertainty is 5%. The results were normalized to the ETH standard S555N (33).

Computational Analysis. The radionuclide records were combined into one using principal component analysis (PCA) to obtain a record covering the entire period of interest. First we divided each record into a series of consecutive 22-year intervals, with the interval centers being the same for all records. The data points in each interval were averaged, and this average was assigned to the central age. The principal components (PCs) were built from eight blocks of records with each block containing two to six individual radionuclide records (*SI Appendix*, Section S6). The first PC describes most of the total variance and is interpreted as the production signal due to solar and geomagnetic modulation. The first PC of one block is then normalized in such a way that its mean is equal to the mean of the first PC of the previous block in the overlapping interval covered by the two blocks. Note that we changed only the mean but not the variance. Finally, the curves of the eight blocks are combined to represent the common production signal variation. The robustness was tested with a jackknife method by repeating PCA and systematically leaving out one radionuclide record.

ACKNOWLEDGMENTS. We acknowledge financial support by National Centre of Competence in Research climate, Swiss climate research, and by the Swiss National Science Foundation under Grant CRSI122-130642 (Future and Past Solar Influence on the Terrestrial Climate). This work is a contribution to the European Project for Ice Coring in Antarctica (European Project for Ice Coring in Antarctica), a joint European Science Foundation/European Commission scientific program, funded by the European Union and by national contributions from Belgium, Denmark, France, Germany, Italy, the Netherlands, Norway, Sweden, Switzerland, and the United Kingdom. The main logistic support was provided by L'Institut polaire français Paul-Emile Victor and Programma Nazionale di Ricerche in Antartide (at Dome C) and Alfred-Wegener Institute (at Dronning Maud Land). This is EPICA publication no. 282.

1. McCracken KG, Beer J (2007) Long-term changes in the cosmic ray intensity at Earth, 1428–2005. *J Geophys Res-Space* 112:A10101.
2. Beer J (2000) Neutron monitor records in broader historical context. *Space Sci Rev* 107–119.
3. Masarik J, Beer J (2009) An updated simulation of particle fluxes and cosmogenic nuclide production in the Earth's atmosphere. *J Geophys Res-Atmos* 114:D11103.
4. Siegenthaler U (1983) Uptake of excess CO_2 by an outcrop-diffusion model of the ocean. *J Geophys Res-Oc Atm* 88:3599–3608.
5. Beer J, McCracken KG, Abreu J, Heikkilä U, Steinhilber F (2011) Cosmogenic radionuclides as an extension of the neutron monitor era into the past: potential and *Limitations Space Sci Rev.* ONLINE FIRST ARTICLE.
6. Fischer H, Siggaard-Andersen ML, Ruth U, Rothlisberger R, Wolff E (2007) Glacial/interglacial changes in mineral dust and sea-salt records in polar ice cores: Sources, transport, and deposition. *Rev Geophys* 45:RG1002.
7. Solanki SK, Usoskin IG, Kromer B, Schussler M, Beer J (2004) Unusual activity of the Sun during recent decades compared to the previous 11,000 years. *Nature* 431:1084–1087.
8. Steinhilber F, Abreu J, Beer J (2008) Solar modulation during the Holocene. *Astrophysics and Space Sciences Transactions* 4:1–6, (http://www.astrophysics-and-space-sciences-transactions.net/).
9. Usoskin IG, Solanki SK, Kovaltsov GA (2007) Grand minima and maxima of solar activity: new observational constraints. *Astron Astrophys* 471:301–309.
10. Vonmoos M, Beer J, Muscheler R (2006) Large variations in Holocene solar activity: Constraints from Be-10 in the Greenland Ice Core Project ice core. *J Geophys Res-Space* 111:A10105.
11. Abreu JA, Beer J, Steinhilber F, Christl F, Kubik PW (2012) ^{10}Be in Ice Cores and ^{14}C in tree rings: separation of production and climate effects. *Space Sci Rev* ONLINE FIRST ARTICLE.
12. Muscheler R, et al. (2004) Changes in the carbon cycle during the last deglaciation as indicated by the comparison of Be-10 and C-14 records. *Earth Planet Sc Lett* 219:325–340.
13. Yiou F, et al. (1997) Beryllium 10 in the Greenland Ice Core Project ice core at Summit, Greenland. *J Geophys Res-Oceans* 102:26783–26794.
14. Reimer PJ, et al. (2009) Intcal09 and Marine09 radiocarbon age calibration curves, 0–50,000 Years Cal Bp. *Radiocarbon* 51:1111–1150.
15. Berggren AM, et al. (2009) A 600-year annual Be-10 record from the NGRIP ice core, Greenland. *Geophys Res Lett* 36:L11801.
16. Beer J, Tobias S, Weiss N (1998) An active sun throughout the Maunder Minimum. *Sol Phys* 181:237–249.
17. Beer J, et al. (1985) Accelerator measurements of Be-10—the 11 Year solar-cycle from 1180–1800 Ad. *Nucl Instrum Meth B* 10-1:415–418.
18. Horiuchi K, et al. (2008) Ice core record of Be-10 over the past millennium from Dome Fuji, Antarctica: a new proxy record of past solar activity and a powerful tool for stratigraphic dating. *Quat Geochronol* 3:253–261.
19. Raisbeck GM, Yiou F, Jouzel J, Petit JR (1990) Be-10 and Delta-H-2 in polar ice cores as a probe of the solar variability influence on climate. *Philos T R Soc A* 330:463–470.
20. Eddy JA (1976) The Maunder minimum. *Science* 192:1189–1202.
21. Knudsen MF, et al. (2008) Variations in the geomagnetic dipole moment during the Holocene and the past 50 kyr. *Earth Planet Sc Lett* 272:319–329.
22. Steinhilber F, Beer J, Frohlich C (2009) Total solar irradiance during the Holocene. *Geophys Res Lett* 36:L19704.
23. Steinhilber F, Abreu JA, Beer J, McCracken KG (2010) Interplanetary magnetic field during the past 9300 years inferred from cosmogenic radionuclides. *J Geophys Res-Space* 115:A01104.
24. Frohlich C (2009) Evidence of a long-term trend in total solar irradiance. *Astron Astrophys* 501:L27–U508.
25. Vieira LEA, Solanki SK, Krivova N, Usoskin I (2011) Evolution of the solar irradiance during the Holocene. *Astron Astrophys* 531:A6.
26. Wang YJ, et al. (2005) The Holocene Asian monsoon: links to solar changes and North Atlantic climate. *Science* 308:854–857.
27. LeGrande AN, Schmidt GA (2009) Sources of Holocene variability of oxygen isotopes in paleoclimate archives. *Clim Past* 5:441–455.
28. Abreu JA, Beer J, Ferriz-Mas A (2010) Past and future solar activity from cosmogenic radionuclides. Astronomical Society of the Pacific Conference Series: SOHO-23: understanding a peculiar solar minimum. *SOHO-23: understanding a peculiar solar minimum*, eds SR Cranmer, JT Hoeksema, and JL Kohl 428 (Astronomical Society of the Pacific Conference Series (2010), UT), pp 287–295.
29. Damon PE, Sonett CP (1991) Solar and terrestrial componants of the atmospheric ^{14}C variation spectrum. *The Sun in Time*, eds CP Sonett, MS Giampapa, and S Matthews (University of Arizona Press, Tucson), pp 360–388.
30. Korschinek G, et al. (2010) A new value for the half-life of Be-10 by heavy-ion elastic recoil detection and liquid scintillation counting. *Nucl Instrum Meth B* 268:187–191.
31. Chmeleff J, von Blanckenburg F, Kossert K, Jakob D (2010) Determination of the Be-10 half-life by multicollector ICP-MS and liquid scintillation counting. *Nucl Instrum Meth B* 268:192–199.
32. Epica Community Members (2006) One-to-one coupling of glacial climate variability in Greenland and Antarctica. *Nature* 444:195–198.
33. Kubik PW, Christl M (2010) Be-10 and Al-26 measurements at the Zurich 6 MV Tandem AMS facility. *Nucl Instrum Meth B* 268:880–883.
34. Heikkila U, Beer J, Feichter J (2009) Meridional transport and deposition of atmospheric Be-10. *Atmos Chem Phys* 9:515–527.
35. Ruth U, et al. (2007) EDML1: A chronology for the EPICA deep ice core from Dronning Maud Land, Antarctica, over the last 150,000 years. *Clim Past* 3:475–484.
36. Vinther BM, et al. (2006) A synchronized dating of three Greenland ice cores throughout the Holocene. *J Geophys Res-Atmos* 111:D13102.
37. Rasmussen SO, et al. (2006) A new Greenland ice core chronology for the last glacial termination. *J Geophys Res-Atmos* 111:D06102.
38. Usoskin IG, Bazilevskaya GA, Kovaltsov GA (2011) Solar modulation parameter for cosmic rays since 1936 reconstructed from ground-based neutron monitors and ionization chambers. *J Geophys Res-Space* 116:A02104.
39. SIDC-Team (2012), The International Sunspot Number Monthly Report on the International Sunspot Number, online catalogue, http://www.sidc.be/sunspot-data/.